Journal of Aerosol Science 53 (2012) 40–60

Contents lists available at SciVerse ScienceDirect

Journal of Aerosol Science

journal homepage: www.elsevier.com/locate/jaerosci

Vapor deposition during cigarette smoke inhalation in a subject-specific human airway model

Zhe Zhang [a], Clement Kleinstreuer [a,b,*], Yu Feng [a]

[a] Department of Mechanical and Aerospace Engineering, North Carolina State University, Raleigh, NC 27695, USA
[b] Joint Department of Biomedical Engineering, North Carolina State University, Raleigh, and University of North Carolina, Chapel Hill, NC, USA

ARTICLE INFO

Article history:
Received 27 January 2012
Received in revised form
7 May 2012
Accepted 16 May 2012
Available online 29 May 2012

Keywords:
Cigarette smoke
Respiratory vapor mass transfer and deposition
Transient puffing and inhalation
Subject-specific human upper airways
Computational analysis
Quantitative data sets for toxicologists

ABSTRACT

Validated computer simulation results of vapor deposition from inhaled cigarette smoke are helpful to assess potential health effects of conventional and so-called less-harmful tobacco products. In this paper, the depositions of four critical tobacco-smoke vapors, i.e., acrolein, 1,3-butadiene, acetaldehyde and CO, in a subject-specific human airway model from mouth to generation G9 under different inhalation conditions have been simulated. The results show that vapor deposition is strongly influenced by its property values as well as inhalation waveform, i.e., puffing behavior. As almost insoluble species in the mucus layer, the deposition of butadiene vapor and CO is very low in the upper airways. The remaining vapors may penetrate further and deposit in deeper lung regions. As medium-to-high soluble vapors, acrolein and acetaldehyde have very high deposition values in the human upper airways from mouth to generation G9. The deposition result for steady matching flow (where the average flow rate between mean and peak values was taken) is a good conservative estimate of the actual deposition fraction under transient normal inhalation condition. However, the vapor transport delay may largely reduce the vapor deposition for transient puffing. A correction factor has been proposed, considering vapor transport delay, in order to calculate efficiently actual deposition fraction values under transient puffing condition. Furthermore, the effect of different puffing waveforms for conventional cigarettes and PREPs (potential reduced exposure products) on smoke vapor deposition has been discussed as well. Finally, a set of deposition correlations have been developed to estimate the deposition of acrolein and acetaldehyde vapors in different segments of the human upper airways under both puffing and normal inhalation (i.e., post-puffing) conditions.

1. Introduction

Tobacco-smoking can be addictive, with potentially detrimental effects and related high health-care cost. So far, more than 60 carcinogens have been detected in mainstream smoke of cigarettes and most of the same carcinogens are present in sidestream smoke. Hecht, (2002, 2003), Burns et al. (2008) and Hecht et al. (2010) summarized the most important carcinogens in cigarette-smoke compounds, i.e., acetaldehyde, acrolein, benzene, benzo[*a*]pyrene (BaP), 1,3-butadiene, carbon monoxide (CO), ethylene oxide, cadmium, 4-aminobiphenyl, formaldehyde, NNN, and NNK. Some of these toxicants

* Corresponding author at: Department of Mechanical and Aerospace Engineering, North Carolina State University, NC 27695-7910, USA. Tel.: +1 919 515 5261; fax: +1 919 515 7968.
E-mail address: ck@ncsu.edu (C. Kleinstreuer).

0021-8502/$ - see front matter © 2012 Elsevier Ltd. All rights reserved.
http://dx.doi.org/10.1016/j.jaerosci.2012.05.008

(e.g., acetaldehyde, acrolein, 1,3-butadiene, CO) inhaled from cigarettes appear as gas/vapor. Hence, the deposition doses of such vapors in human lungs are directly linked to the harmful effect of tobacco smoking. In addition, the recent appearance of potential reduced exposure products (PREPs) is a step to reduce harm of tobacco products (cigarettes); but, the validity of that claim requires careful testing (Laugesen & Fowles, 2006; Lin et al., 2010; Zhang et al., 2012). In fact, PREPs with tobacco reconstitution and new device designs may also alter a smoker's puffing behavior, which can also change the lung deposition patterns of smoke vapors when compared to conventional cigarettes. Hence, tracking and computing the intake and deposition of toxic vapors of both PREPs and conventional cigarettes during transient puffing and post-puffing is also helpful to test the "less-harmful-cigarette" claim of PREPs and to provide toxicologists with reliable quantitative data sets. Furthermore, as many inhaled toxic or drug aerosols may appear partially in vapor form, validated computer simulation of local and regional uptake dosage of vapors in the respiratory tract would provide vital information for pharmacokinetic modeling.

As reviewed by Baker & Dixon (2006), very limited information has been published on the retention of vapors from cigarette smoke. Tolman (1973) measured the retention of carbon monoxide as a function of breathing patterns and hold time and found that the total retention of CO increased from 37% to 82% with holding time from 0.3 s to 60 s. Backhurst & Martin (1973) measured a range of smoke vapors in different subjects during puffing. They reported very high total lung retentions of acetaldehayde vapor ($>94\%$) and acrolein vapor ($>97\%$). However, local and regional deposition data of smoke vapors in human lungs are not available. More experimental studies on vapor deposition focused on laboratory animals. For example, Morris & Blanchard (1992) and Morris (1996, 1997), using rats and other animals, measured the uptake of inhaled acrolein and acetaldehyde vapor. They detected high-level deposition of these two vapors in the URT (upper respiratory tract) of such rodents. The results also indicated that the average URT acrolein deposition efficiency was significantly dependent on the inspired concentration when such concentrations are higher than 2 m μg/L (0.87 ppm) for acrolein and 1 ppm for acetaldehyde. However, the realistic human exposure level is usually lower (say, <1 ppm). Hence, the measured dosimetry data for animals under high-exposure scenarios cannot be directly extrapolated to humans.

1-D mathematical modeling and 3-D computational fluid dynamics (CFD) simulations are alternative approaches to obtain deposition data of vapors in human lungs. 1-D mathematical modeling for steady or unsteady diffusion of vapors usually assumes uniform airflow in the airway lumen (see Asgharian et al., 2011) and hence ignores the effects of 3-D airway geometries. 3-D CFD simulations have been recently conducted in human upper airways or for isolated lung segments (see Keyhani et al., 1997; Bush et al., 1998; Zhao et al., 2004; Zhang et al., 2006; Morris & Hubbs, 2009; Tian & Longest, 2010a,b; Zhang & Kleinstreuer, 2011a,b,c; among others). Most recently, Zhang et al. (2012) simulated the transport and deposition of size-changing nanodroplets in a realistic human upper airway model under different steady inhalation conditions. Comparisons of local exposure-dose values between conventional and possibly less-harmful cigarettes are provided. Nevertheless, studies so far considered just steady or simple inhalation waveforms for particle transport. Thus, the effects of transient puffing as well as different realistic inhalation waveforms on vapor deposition in actual human airways have not been investigated.

In this paper, the transient depositions of smoke vapors in a subject-specific human upper airway model from mouth to G9 during puffing and post-puffing have been simulated. Four important carcinogens in cigarette-smoke compounds, i.e., acrolein, 1,3-butadiene, acetaldehyde and CO were selected as the species for gas/vapor transport/deposition studies. These four compositions released from cigarettes appear mostly in the gas phase at the mouth inlet (PMP, 2010). A comparison of vapor deposition between PREP puffing and conventional cigarette (CC) puffing has been conducted as well.

2. Methods

2.1. Background information

Both the human airway geometry and the airflow dynamics are described in Zhang et al. (2012). Briefly, the in-house subject-specific human respiratory system encompasses the mouth (with an 8 mm opening simulating the cigarette) to generation G9 of the tracheobronchial airways (see Fig. 1). The subject for this study is a 47-year old healthy male volunteer, 174 cm of height and 78 kg of weight. The subject does not have any history of respiratory diseases. This airway model was fully constructed from high-resolution CT-images. Specifically, GE's 64-slice CT scanner was used to take images of 500 mm by 500 mm (i.e., 512∗512 pixels on the plane) cross-sections with 2.5 mm slice thickness from the extra-cranial skull base to the abdominal region of the subject. In-between slices were created via an interpolation process.

During the scan, an 8-mm circular tube was inserted into the front middle part of the mouth of the subject to mimic cigarette-smoking while the subject was breathing through the mouth only. During inhalation, the subject was asked to lower the tongue to create a passage for the air through the oral cavity. At the end of inhalation, the subject stopped breathing but was asked to keep the airway passage through the pharynx and larynx open. ScanIP software (image processing software, Simpleware Inc., Exeter, UK) was employed to select and reconstruct the regions of interest. The stereo-lithography file (STL file) generated by ScanIP was imported into ICEM CFD (i.e., mesh generation software from ANSIS, Inc.) to create the computational mesh.

The airflow dynamics of the respiratory tract is always unsteady and driven by the pressure differences under the action of the cyclic breathing process. The incompressible Navier–Stokes (NS) equations were employed to characterize airflow primarily in this study. During puffing, the inhalation flow rate is low (say, $Q_{in}<80$ mL/s), the maximum Reynolds number in human airways is less than 800 and hence the flow should be laminar. However, during the post-puffing period

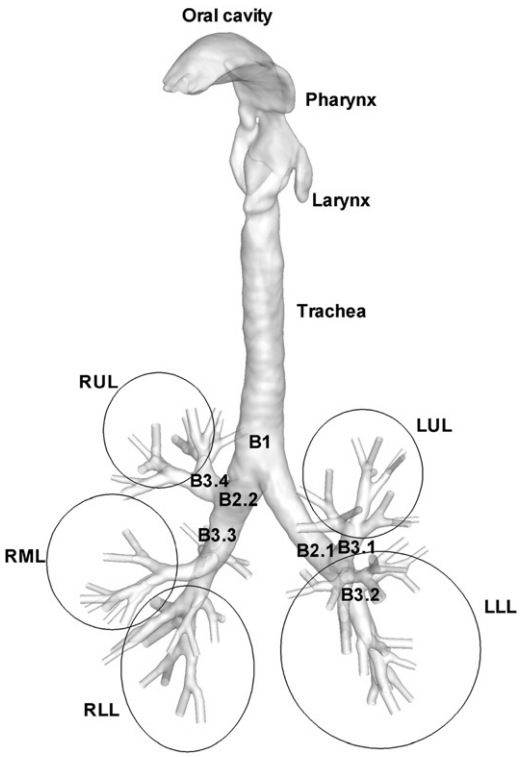

Fig. 1. Configuration of a subject-specific human airway model. Note that LUL to RUL only refer to the corresponding airway braches for deposition calculations.

and at normal breathing rates, the local Reynolds numbers range from 0 to 10,000; hence, airflow through the oral airway region and first few generations is incipient turbulent, becoming laminar at about the sixth to eighth generation, and remaining so thereafter. In order to capture the airflow structures in the laminar-to-turbulent flow regimes, a modified version of the transitional shear-stress-transport (SST) model was selected (Zhang & Kleinstreuer, 2011b). For the SST transition model two additional transport equations, i.e., one for the intermittency and one for the transition-onset criterion in terms of the momentum-thickness Reynolds number, were introduced for a wide range of transitional flows (Menter et al., 2006a,b). Recently, Tan et al. (2008) demonstrated that a correlation-based transitional version of Menter's SST-transition model achieved a good overall agreement with experimental data for pulsatile flow in an axisymmetrically restricted tube. Our simulations also demonstrated that the transitional SST-model can predict mean velocity distributions and turbulence kinetic energy profiles accurately for laminar-transitional-turbulent flow (Zhang & Kleinstreuer, 2011b). The corresponding turbulence equations can be found in Menter et al. (2006a,b) as well as in Zhang & Kleinstreuer (2011b).

Uniform velocity profiles were prescribed at the mouth inlet (see Fig. 1), and a uniform pressure was assumed at the outlets. Exit tubes were extended a few tube diameters from the terminal bifurcation-ends to reduce the influence of the zero-pressure assumption at the outlet. Based on prescribed flow rates and the impedances of the small airway trees downstream, Ma & Lutchen (2006) reported that pressures at the 13 outlets of an anatomically based G-6 airway model were very close to each other. Moreover, the lobar ventilation rate ratios (i.e., LUL:LLL:RLL:RML:RUL as indicated in Fig. 1) for $Q=30$ L/min obtained with the present simulation assuming uniform outlet pressures are 0.183: 0.255:0.287:0.095:0.180. These findings are quite close to the values given by Horsfield et al. (1971) for a normal subject, i.e., 0.205:0.249:0.232:0.096:0.217. Zhang & Kleinstreuer (2011c) also investigated the impact of different outlet flow-rate ratios on vapor/nanoparticle deposition in bronchial airways and found that different outlet pressures primarily influence the velocity profiles and vapor/nanoparticle deposition fractions at that particular branch and adjacent bifurcations. In addition, the impact of change in outlet flow-rate ratio on total deposition was confined to all same-level bifurcations and direct upstream-level bifurcations. Lung compliance or lung motion may influence lobar flow, which will be part of future studies.

2.2. Vapor transport and airway wall uptake

The vapor mass transfer equation, including turbulent dispersion, can be written as:

$$\frac{\partial Y}{\partial t}+\frac{\partial}{\partial x_j}(u_j Y)=\frac{\partial}{\partial x_j}\left[\left(\tilde{D}_a+\frac{v_T}{\sigma_Y}\right)\frac{\partial Y}{\partial x_j}\right] \tag{1}$$

where Y is the mass fraction of vapor, $\sigma_Y=0.9$ is the turbulence Schmidt number for Y, and $\tilde{D}_a$ is the molecular diffusivity of vapor in air.

Assuming that the airway wall is a perfect sink for aerosols or vapors upon touch, the boundary condition at the wall is $Y_w=0$. This assumption is reasonable for fast gas-wall reaction kinetics, or vapors of high solubility and reactivity, and also suitable for estimating the maximum deposition of vapors in the airways. For less soluble vapors, the wall concentration would be greater than zero so that transport in tissue and in airways must be considered simultaneously when simulating vapor uptake.

Assuming that the surface of the respiratory epithelium is covered by a mucus layer with uniform thickness and that a lipid layer (tissue) lies below the mucus-tissue interface, representing a transport barrier by the epithelial cell membrane, quasi-steady radial mass transfer in the mucus layer, tissue and blood (capillary) may occur. If the concentration below the lipid compartment is also assumed to be zero with rapid removal of vapor molecules by the underlying tissue, a simplified flux condition at the airway boundary can be given as (Keyhani et al., 1997):

$$\frac{\partial Y}{\partial n}+KY=0 \tag{2a}$$

where n is the direction normal to the airway wall and K is called as wall absorption coefficient. It is defined as:

$$K=\frac{\tilde{D}_m\xi}{\tilde{D}_a\beta\tanh(\xi H_m)}\left[1-\frac{2\tilde{D}_m/H_m}{(\tilde{D}_m/H_m+P_l)(e^{\xi H_m}-e^{-\xi H_m})}\right] \tag{2b}$$

where $\tilde{D}_a$, $\tilde{D}_m$ are the vapor diffusivity in the air and the liquid mucus phase, respectively; H_m is the thickness of the mucus layer; and β is the equilibrium partition coefficient for a given contaminant molecule, which can be determined by Henry's law; $\xi=\sqrt{k_r/\tilde{D}_m}$ with k_r being a single rate constant considering the chemical reactions of vapors in the mucus layer; $P_l=\gamma\tilde{D}_l/H_l$ is the lipid permeability coefficient with γ,$\tilde{D}_l$,H_l being lipid-mucus partition coefficient, vapor diffusivity in the lipid and the thickness of the lipid layer, respectively.

The saturable pathway elimination for absorbed vapors in the mucus-tissue layer may also influence vapor deposition (Teeguarden et al., 2008). Considering the effect of saturable elimination pathway, the tissue transport reactive-diffusion equation is formulated as:

$$\frac{\partial Y_t}{\partial t}=\tilde{D}_t\frac{\partial^2 Y_t}{\partial n^2}-K_fY_t-\frac{(V_{\max}/V_t)Y_t}{K_m+Y_t} \tag{3a}$$

where the layers of mucus and tissue are considered as one "tissue" layer; Y_t and $\tilde{D}_t$ are vapor concentration and diffusivity in the tissue, respectively; K_f is the first-order elimination rate constant; K_m and $V_{\max}$ are the Michaelis–Menten parameters, and V_t is tissue volume. Asgharian et al. (2011) proposed an approximate approach to simplify the curve of saturable pathway elimination rate by two bounding lines. When the tissue vapor concentration is below the saturable plateau, i.e., $Y_t\le Y_t^*$ (Y_t^* is the maximum tissue concentration in the saturable pathway, and $Y_t^*\approx K_m$), Eq. (3a) can be rewritten as:

$$\frac{\partial Y_t}{\partial t}=\tilde{D}_t\frac{\partial^2 Y_t}{\partial n^2}-\left(K_f+\frac{V_{\max}}{K_mV_t}\right)Y_t \tag{3b}$$

When tissue concentration is greater than the saturable plateau ($Y_t>Y_t^*$), Eq. (3b) becomes:

$$\frac{\partial Y_t}{\partial t}=\tilde{D}_t\frac{\partial^2 Y_t}{\partial n^2}-\left(K_f+\frac{V_{\max}}{K_mV_t}\right)Y_t \tag{3c}$$

The analytical solutions of unsteady vapor concentrations in the tissue are also given by Asgharian et al. (2011). For the quasi-steady case, the boundary condition at the air-tissue interface for $Y_t>Y_t^*$ can be still represented by Eq. (2a) when using

$$K=\frac{\tilde{D}_t\sqrt{\overline{K}_f/\tilde{D}_t}}{\beta\tilde{D}_a\tanh(H_t\sqrt{\overline{K}_f/\tilde{D}_t})}\quad\text{and}\quad\overline{K}_f=K_f+\frac{V_{\max}}{K_mV_t} \tag{4a, b}$$

However, when $Y_t>Y_t^*$, the boundary condition at air-tissue interface should be

$$\frac{\partial Y}{\partial n}+KY+K_0=0 \tag{5a}$$

where

$$K=\frac{\tilde{D}_t\sqrt{K_f/\tilde{D}_t}}{\beta\tilde{D}_a\tanh(H_t\sqrt{K_f/\tilde{D}_t})} \tag{5b}$$

and

$$K_0 = \frac{V_{\max}}{\tilde{D}_a V_t \sqrt{K_f/\tilde{D}_t}} \left[\frac{1}{\tanh\left(H_t\sqrt{K_f/\tilde{D}_t}\right)} - \frac{1}{\sinh\left(H_t\sqrt{K_f/\tilde{D}_t}\right)} \right] \tag{5c}$$

It can be expected from the boundary conditions (2a) and (5a) that vapor absorption at the airway surface is greatly influenced by the absorption coefficient K. Clearly, for vapors of different species the absorption coefficient K should be different as well. Although actual vapor absorption in the mucus-tissue-blood system is transient, the quasi-steady conditions (2a) and (5a) represent conservative, i.e., possibly maximum, vapor depositions at the airway surface. The comparison between the present quasi-steady boundary conditions and more realistic transient absorption as well as the limitation of such somewhat simplified boundary conditions is discussed in Sections 3.7 and 3.8.

2.3. Calculation of vapor deposition

Evaluation of injuries from inhalation exposure to toxic vapors requires a detailed knowledge of the deposited amount and distribution of toxins in the human airways. The inhaled dose of vapors is described by the deposition fraction (DF) or deposition efficiency (DE), which can be calculated by summing up local wall mass fluxes. The local wall mass flux of vapors can be determined as:

$$\dot{m}_w = -\rho A_i \left(\tilde{D}_a + \frac{v_T}{\sigma_Y}\right)\left.\frac{\partial Y}{\partial n}\right|_i \tag{6}$$

where A_i is the area of the local wall cell (i). The local vapor deposition fraction or deposition efficiency, which is defined as the ratio of local wall mass flux to the mass flux at mouth inlet or local inlet of the airway segment, can be expressed as:

$$DF_{local} = (A_i j_{wall,i})/(Q_{mouth,in} Y_{mouth,in}) \tag{7a}$$

$$DE_{local} = (A_i j_{wall,i})/(Q_{local,in} Y_{local,in}) \tag{7b}$$

The *regional DF* or DE can be determined as:

$$DF_{region} = \sum_{i=1}^{n} (A_i j_{wall,i})/(Q_{mouth,in} Y_{mouth,in}) \tag{7c}$$

$$DE_{region} = \sum_{i=1}^{n} (A_i j_{wall,i})/(Q_{local,in} Y_{local,in}) \tag{7d}$$

where n is the number of wall cells in one specific airway region, e.g., oral airway, first airway bifurcation, etc. The subscript "mouth, in" refers to mouth inlet, while "local, in" refers to the inlet at the specific airway bifurcation. The local inlet flow rate and particle mass are calculated as the sum of local values of cells at this specific inlet.

The local vapor deposition patterns can be quantified in terms of a deposition enhancement factor (DEF), which is defined as the ratio of local to average deposition densities, i.e.,

$$DEF = \left[\left(\tilde{D} + \frac{v_T}{\sigma_Y}\right)\left.\frac{\partial Y}{\partial n}\right|_i\right] \Big/ \left\{\sum_{i=1}^{n}\left[A_i\left(\tilde{D} + \frac{v_T}{\sigma_Y}\right)\left.\frac{\partial Y}{\partial n}\right|_i\right] \Big/ \sum_{i=1}^{n} A_i\right\} \tag{8}$$

DEF indicates vapor deposition "hot spots" in a given region.

2.4. Calculation of mass transfer coefficients

Calculation of the respiratory mass transfer coefficient, h_m, is helpful in quantitatively predicting the regional deposition of inhaled vapors (Kleinstreuer & Zhang, 2010). The relationship between the deposition efficiency (DE) in an airway segment and a given h_m can be described as (Zhang & Kleinstreuer, 2011a):

$$DE = 1 - \frac{Y_{out}}{Y_{local,in}} = 1 - \exp\left(-\frac{h_m D_p K}{h_m + D_p K} \cdot \frac{A_s}{Q_{local,in}}\right) \tag{9a}$$

Clearly, the DE for $K=0$ is equal to zero, and for $K \to \infty$, Eq. (9a) reduces to

$$DE = 1 - \exp\left[\frac{-h_m A_s}{Q_{local,in}}\right] \tag{9b}$$

With simulated DE-values, the mass transfer coefficient for one airway segment can be determined from Eq. (9) as well. The Sherwood number (Sh), representing the ratio of convective to diffusive mass transport, can be expressed as:

$$Sh = (h_m D)/D_p \tag{10}$$

where D is the characteristic diameter of the airway segment. Necessary physical property values for the vapors of interest are listed in Table 1.

2.5. Numerical method

The numerical solutions of the governing equations subject to appropriate boundary conditions were carried out with a user-enhanced, commercial finite-volume based program, i.e., CFX12.1 from ANSYS Inc. The computational mesh was generated with Ansys ICEM-CFD. A multi-layer region consisting of dense hybrid tetrahedral/pentahedral elements was generated near the wall surface to fully contain the viscous sub-layers and to resolve any geometric features present there. Such high local mesh resolution is also necessary to accurately calculate near-wall derivative values, such as the deposition fluxes. The mesh topology was determined by refining the mesh until grid independence of the flow field solution and vapor deposition fractions was achieved.

The computations were performed on a local Dell workstation with 12GB RAM and four 3.0 GHz CPUs as well as the multi-processor IBM Blade Center at NCSU HPC (where 32–64 processors were used for this study). The solution of the flow field was assumed to be converged when the dimensionless mass residual was negligible, i.e., (Total Mass Residual)/(Mass Flow Rate) $< 10^{-4}$. The convergence of other variables was monitored as well. Typical run times for the steady air and vapor flow were approximately 72–96 CPU hours and about 1000–1500 CPU hours for a single puffing period.

3. Results and discussion

3.1. Model validations

It is impossible to directly validate the transport and deposition of the selected vapors in the human respiratory tract because there are no relevant measured data available. Instead, the current simulation approach for species-mass deposition due to diffusional transport has been validated via analytical solutions in straight pipes, experimental data for a multi-bifurcation airway model as well as experimental data in the nasal airway model and tracheobronchial airways (see Shi et al., 2008; Zhang et al., 2008; Zhang & Kleinstreuer, 2011b). Fig. 2 depicts another validation example, which is for iodine vapor deposition in a tracheobronchial airway model. Specifically, Li et al. (1998) measured the deposition of iodine

Table 1
Physical properties of selected vapors and gases (at 25 °C and 1 atm).
Sources: http://www.nj.gov/dep/srp/guidance/rs/chemproperties.pdf, Sung M., & Kato S. et al., 2010: *Building & Environment 45*: 2002–2007, http://www.depreportingsvcs.state.pa.us/ReportServer/Pages/ReportViewer.aspx?%2fCPP%2fChemicals, Robert Elliott & Harry Watts, *Canadian Journal of Chemistry*, 1972, *50*:31–34.

	$\tilde{D}_a$ ($cm^2\ s^{-1}$)	$\tilde{D}_m$ ($cm^2\ s^{-1}$)	β	K (cm^{-1}) [a]
Acrolein	0.105	1.22e−5	1.77e−4–5.5e−3 (4.92e−3)	21.1–656 (23.6)
1,3-butadiene	0.1158 [4]	9.5e−6	2.5–103 (2.5)	8e−4–0.0328 (0.0328)
Acetaldehyde	0.124[3]	1.41e−5	3.18e−3–6.92e−3 (3.18e−3)	16.4–35.8 (35.8)
CO	0.19	1.9e−5	43	2.33e−3

[a] The removal of contaminant molecules in the mucus by chemical reaction and the resistance to transport across the lipid barrier are ignored, and the absorption parameter K is approximately calculated as $K = \tilde{D}_m/\tilde{D}_a\beta H_m$ with $H_m = 1 \times 10^{-3}$ cm.

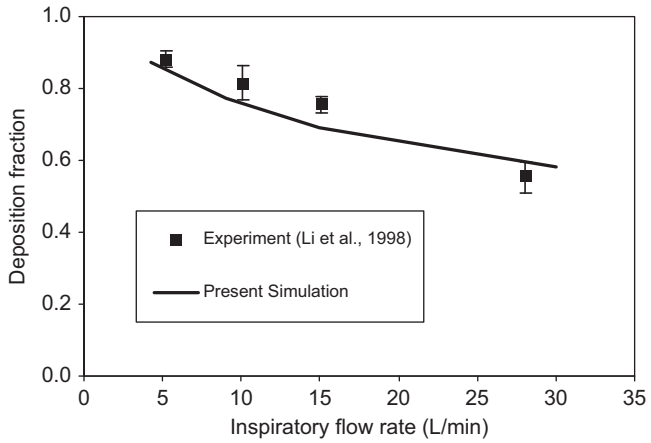

Fig. 2. Comparison of vapor (iodine) deposition fractions based on the present simulation results and experimental measurements in tracheobronchial airways.

vapor in a replicate cast from the trachea (G0) to generation nine (G9) for flow rates between 5 and 30 L/min. It can be seen that simulated depositions based on the present airway configuration from G0 to G9 (i.e., without the oral airway) are in very good agreement with the measurements. Any discrepancies can be attributed to: (i) different airway geometries; and (ii) the lack of an oral airway in the cast model for the experiments.

In summary, the good agreements between independent observations and numerical predictions instill confidence that the present computer simulation model can accurately predict vapor transport and deposition in three-dimensional human airways.

3.2. Vapor deposition under steady puffing and normal inhalation conditions

As indicated via Eqs. (2) and (5), mass transport of vapors in the mucus-tissue system greatly influence vapor deposition form the air stream onto the airway wall. In this study, Sections 3.2–3.6 focus on vapor transport and deposition in the mucus layer under both transient and steady puffing/inhalation, where the relatively simplified boundary conditions (2a) and (2b) were employed. The impact of saturable pathway elimination (i.e., boundary conditions (2a), (4) and (5)) and transient uptake of vapors in the mucus-tissue-blood system are discussed in Sections. 3.7 and 3.8.

3.2.1. Typical vapor deposition values

Clearly, the degree of local vapor absorption by the airway wall influences downstream vapor transport and deposition. For most vapors, the absorption parameter K in Eq. (2b) may fall into a very large value range (e.g., $1\times10^{-4}<K<1000\ \mathrm{cm}^{-1}$) because of the variations in mucus-layer thickness and physical species properties. Nevertheless, $K_{\mathrm{acrolein}}=23.6\ \mathrm{cm}^{-1}$, $K_{\mathrm{butadiene}}=0.0328\ \mathrm{cm}^{-1}$, $K_{\mathrm{acetaldehyde}}=35.8$ and $K_{\mathrm{CO}}=2.33\times10^{-3}\ \mathrm{cm}^{-1}$ are representative values for the human upper airways (see Table 1).

The total deposition fractions of the selected four vapors in the upper airways, incorporating the representative wall absorption conditions, are shown in Fig. 3a. In this case, steady puffing with inspiratory flow rates of 37.5 mL/s and 60 mL/s, post-puffing with inhalation flow rate of 500 mL/s and two-step inhalation were considered. The inhalation flow rate of $Q=2.25$ L/min (37.5 mL/s) is the mean value of a typical puffing action of one particular PREP (PMP, 2010), while $Q=30$ L/min represents the normal inhalation, or post-puffing, flow rate. Inhalation of cigarette-smoke aerosols is usually a two-step process, consisting of puffing followed by normal inhalation (post-puffing), as pointed out by Dickens et al. (2009). During puffing, the soft palate (or glottis) is closed for most smokers; however, some smokers directly inhale the aerosols into the lung (Bernstein, 2004). In this study, steady puffing and normal inhalation refer to the latter (presumably worst) case, so that the aerosols are assumed to be inhaled directly into the lung. The simulations for the combined two-step smoking process were also conducted for comparison. Clearly, the impact of airway wall absorption (or vapor solubility) can be vital for vapor

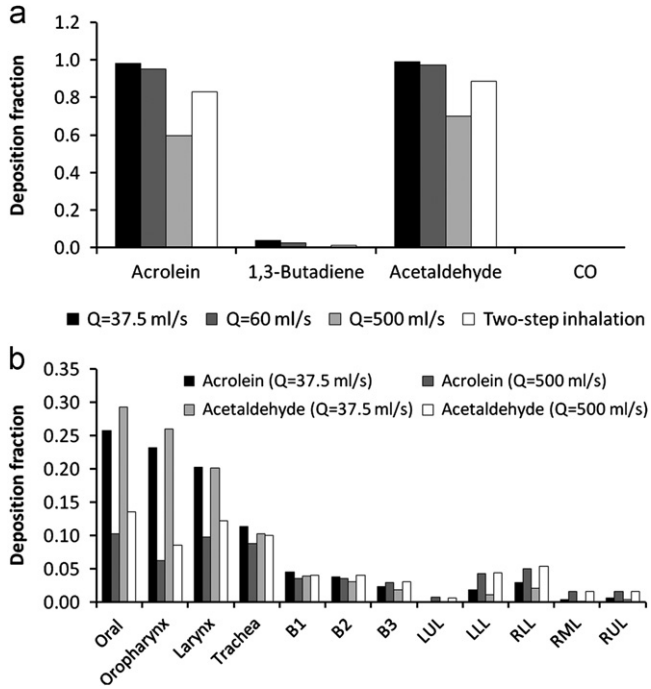

Fig. 3. Vapor deposition in the upper airway model (steady state): (a) Total deposition fraction; and (b) regional deposition fractions.

deposition in human upper airways. As medium-to-high soluble vapors, acrolein and acetaldehyde almost completely deposit in the human upper airways from the mouth to generation G9 under steady puffing conditions (i.e., the total deposition fractions are larger than 98%). In contrast, as almost insoluble species in the mucus layer, the deposition of butadiene vapor and CO is very low in the upper airways, i.e., actually $DF_{\text{butadiene}}=0.026$ and $DF_{\text{CO}}=0.0032$ at $Q=60$ mL/s. The remaining vapors may penetrate further and deposit in deeper lung regions. In fact, with the reduction of mucus layer thickness (H_m) in the lower airways and alveolar regions (say, $H_m \rightarrow 0.1$ μm in the alveolar regions), the increased absorption coefficient (K) may result in enhanced deposition of butadiene vapor and CO in the deeper lung areas. Still, it can be expected that the butadiene vapor and CO depositions are much lower than those of acrolein and acetaldehyde.

The local deposition fractions (DFs) for acrolein and acetaldehyde vapors are depicted in Fig. 3b. The regional deposition for acrolein and acetaldehyde may gradually decrease from the oral cavity to bifurcation B3 because of the heavy (upstream) deposition, causing lower vapor concentrations at the inlet of each downstream region. The different surface areas of different airway regions also lead to different vapor-deposition values. Usually, an airway region with a relatively large surface area may receive a large portion of absorbed vapors. Influenced by the different airway geometries, surface areas, local flow rates and inlet vapor concentrations, the deposition fractions in individual bifurcations vary as well. For example, in the distal airway branches, RLL receives the highest vapor deposition while LUL has the lowest deposition.

As shown in Fig. 3, the inhalation flow rate and puffing behavior may affect vapor deposition, especially in terms of local depositions. The simulated acrolein vapor deposition fraction ($DF=69\%$) in the oral airway (from mouth to larynx) during puffing ($Q=37.5$ mL/s) is very close to the in vivo measured retention data by Backhurst & Martin (1973) ($DF=72\%$). Backhurst & Martin (1973) also found that almost all acrolein vapor deposits in the human lung (say, $DF>97\%$).

Considering the fact that deposition of CO and butadiene vapor is very low in the airway model from the oral cavity to generation G9, the following analyses will focus on vapors of acrolein and acetaldehyde vapors only.

3.2.2. *Vapor deposition pattern*

Local vapor deposition patterns can be described in terms of distributions of the deposition enhancement factor (DEF, see Eq. (8)). Fig. 4 shows the DEF contours of acrolein vapor in the upper airway model for steady puffing ($Q_{\text{oral, in}}=37.5$ mL/s). Clearly, the deposition patterns are somewhat inhomogeneous. Enhanced deposition may occur at the entrance, anterior part of the oral cavity, the outside bend of the pharynx, throat, and carinal ridges of the first bifurcation because of high degrees of mixing, i.e., large concentration gradients and/or complicated airflows in these regions.

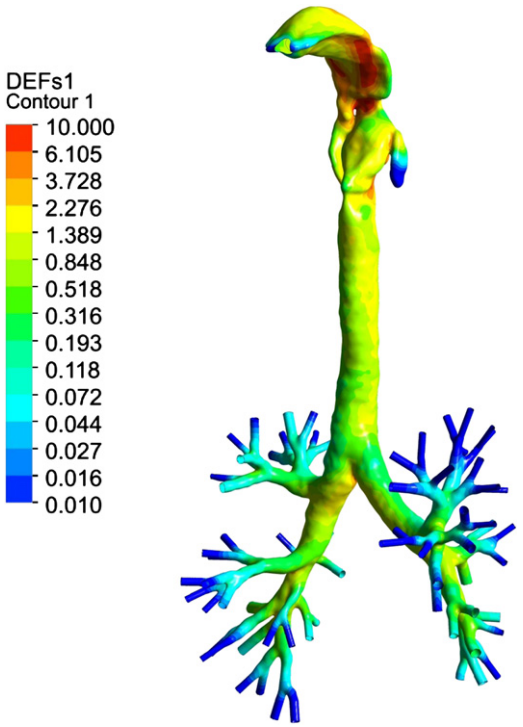

Fig. 4. Vapor deposition (acrolein) pattern in the upper airway model (steady state, $Q=37.5$ mL/s).

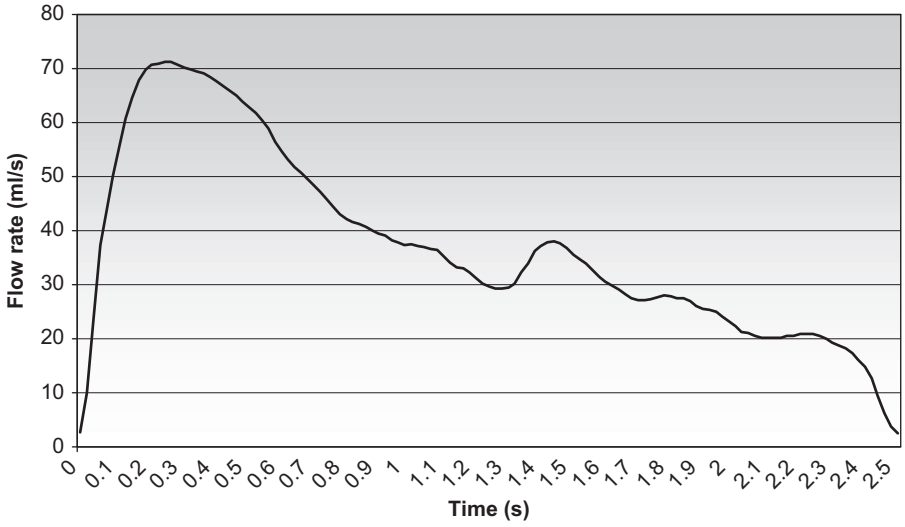

Fig. 5. A typical PREP-puffing waveform (PMP, 2010).

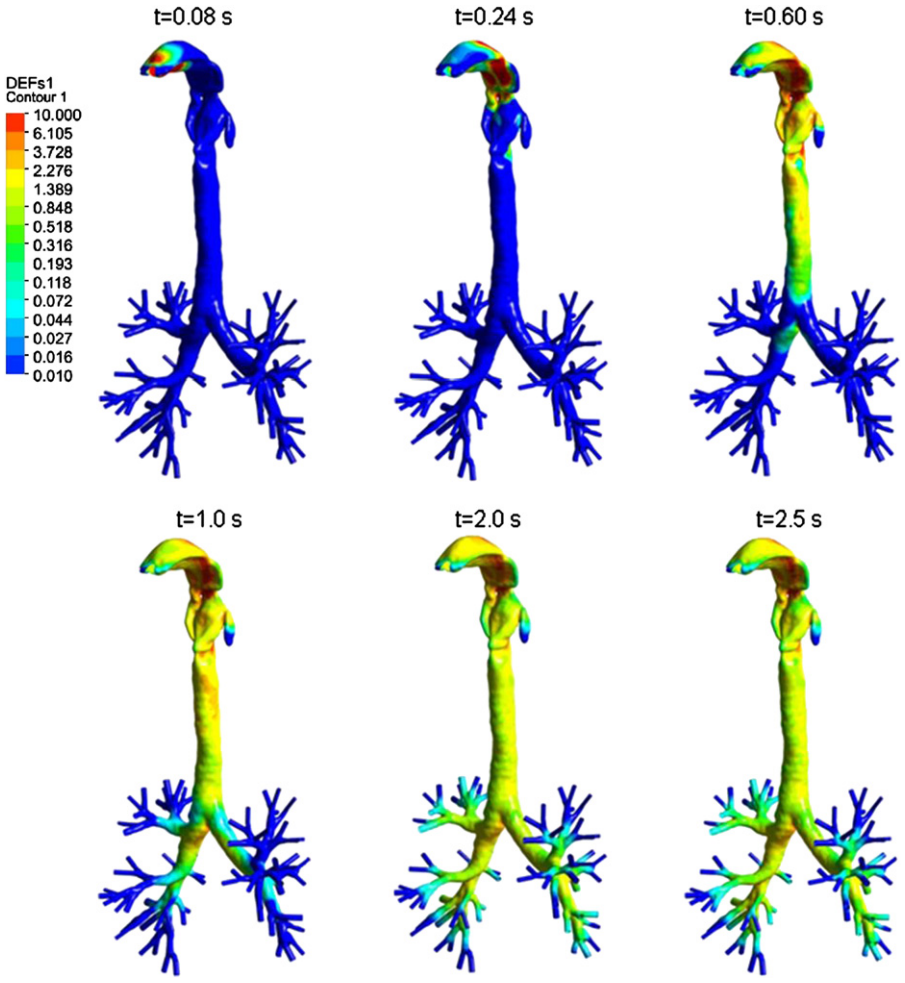

Fig. 6. Transient vapor (acrolein) deposition pattern during puffing period.

3.3. Vapor deposition under transient puffing and inhalation conditions

Realistic inhalation processes during cigarette smoking, including puffing and post-puffing, are transient. The puffing waveforms may vary for different subjects and cigarette brands. As mentioned in the Introduction, the puffing waveforms may change significantly for some PREPs when compared to conventional cigarette smoking. Following the information provided by PMP (2010), Fig. 5 depicts a typical puffing waveform. Thus, possible PREP vapor deposition results under transient puffing and post-puffing (normal inhalation) conditions are discussed next.

Fig. 6 depicts the instantaneous DEF contours of acrolein vapor during the transient PREP-puffing period. As expected, vapor travels and deposits gradually from the mouth inlet to distal branches. The vapor deposition patterns after $t=2.0$ s are very similar to those under steady flow conditions (see Fig. 4).

Fig. 7 shows the variation of momentary deposition fraction (i.e., fraction of deposited mass) during one puffing cycle, which is defined as the ratio of deposited mass at each time interval (0.02 s) to total inhaled mass at the mouth inlet over the entire cycle. As expected, the variation of momentary deposition fraction has a similar trend as the flow rate; because, the inhaled vapor mass at each time level is proportional to the flow rate. However, apparent delays can be observed between deposition and airflow because vapors cannot transport instantaneously into the deeper lung airways, especially

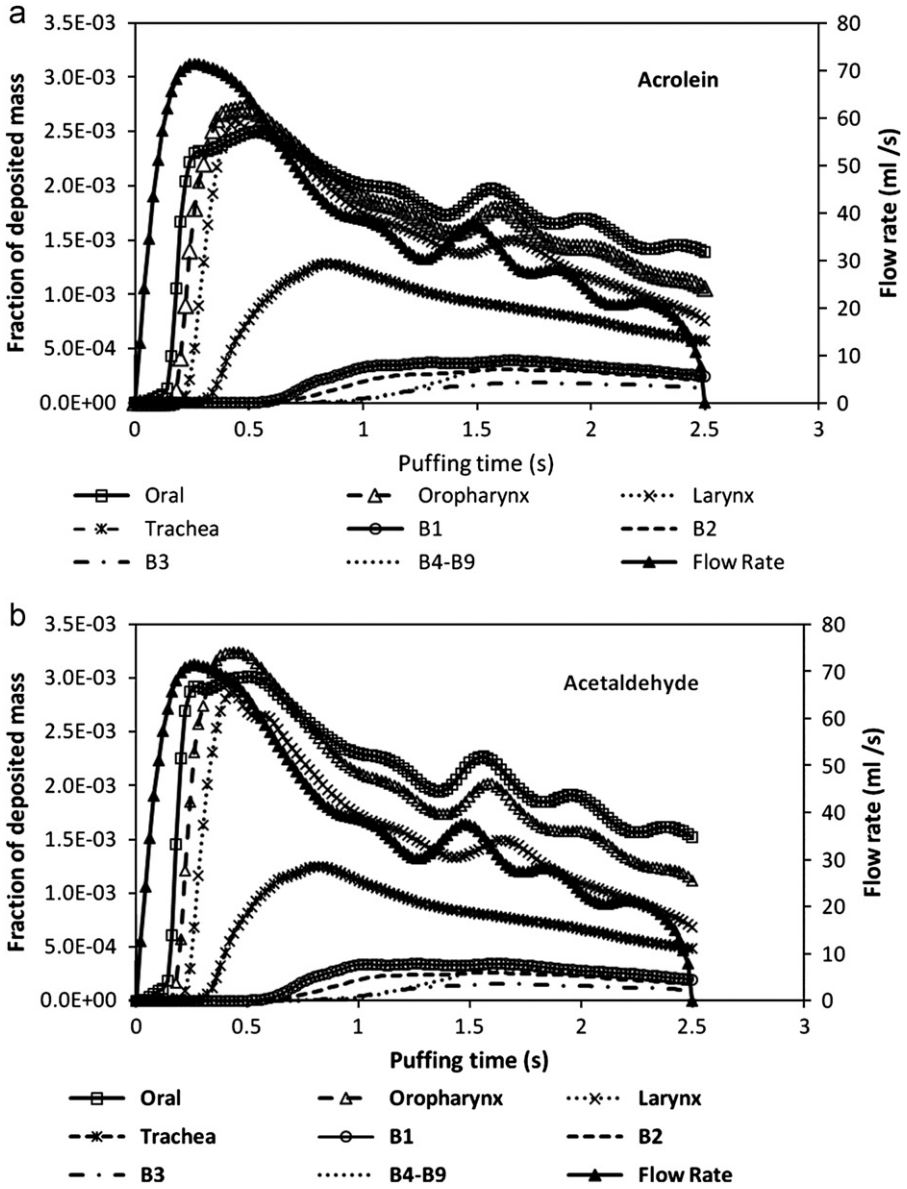

Fig. 7. Variations of momentary deposition fraction during one PREP-puffing cycle: (a) Acrolein vapor deposition in different airway regions; and (b) acetaldehyde vapor deposition in different airway regions.

during puffing at a relatively low flow rate. The delay time into a specific airway segment can be estimated, using the traveling speed and travel distance, as:

$$\int_0^{t_{delay}} \overline{u}(t)dt = L \tag{11}$$

where t_{delay} is the delay time of vapor transport into the specific airway segment, $\overline{u}(t)$ is instantaneous cross-sectionally averaged velocity, and L is the distance starting from the inlet. As shown in Fig. 7, the deeper the extent into the lung, the longer the delay time is. The delay time at different airway regions is given in Table 2, being almost the same for acrolein and acetaldehyde.

Table 2
Transport delay time of vapors in different airway regions.

Region	Oral	Oropharynx	Larynx	Trachea	B1	B2	B3	B4–B9
Delay time (s)	0.06	0.1	0.2	0.32	0.64	0.76	1.02	1.04

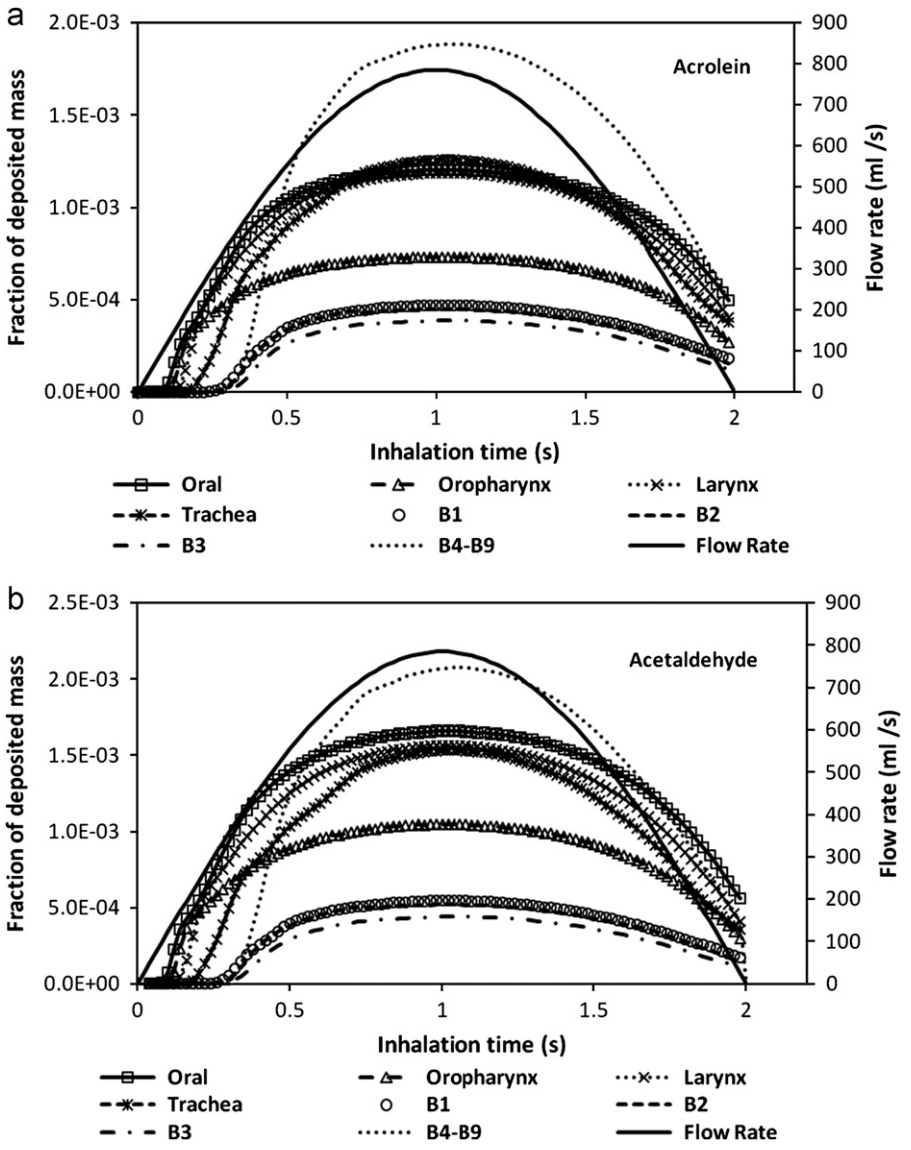

Fig. 8. Variations of momentary deposition fraction during one post-puffing cycle: (a) Acrolein vapor deposition in different airway regions; and (b) acetaldehyde vapor deposition in different airway regions.

Fig. 7 also indicates that the flow rate near the end of inspiration rapidly decreases to zero, but the fraction of deposited mass drops only slightly. This is because of the continuous deposition of lingering vapors occurring over the previous time intervals.

Fig. 8 depicts the variation of momentary deposition fraction during one post-puffing cycle. A sine-wave is assumed for post-puffing (being close to a normal inhalation waveform), i.e.,

$$Q(t) = Q_{max}\sin(\pi t/2) \tag{12}$$

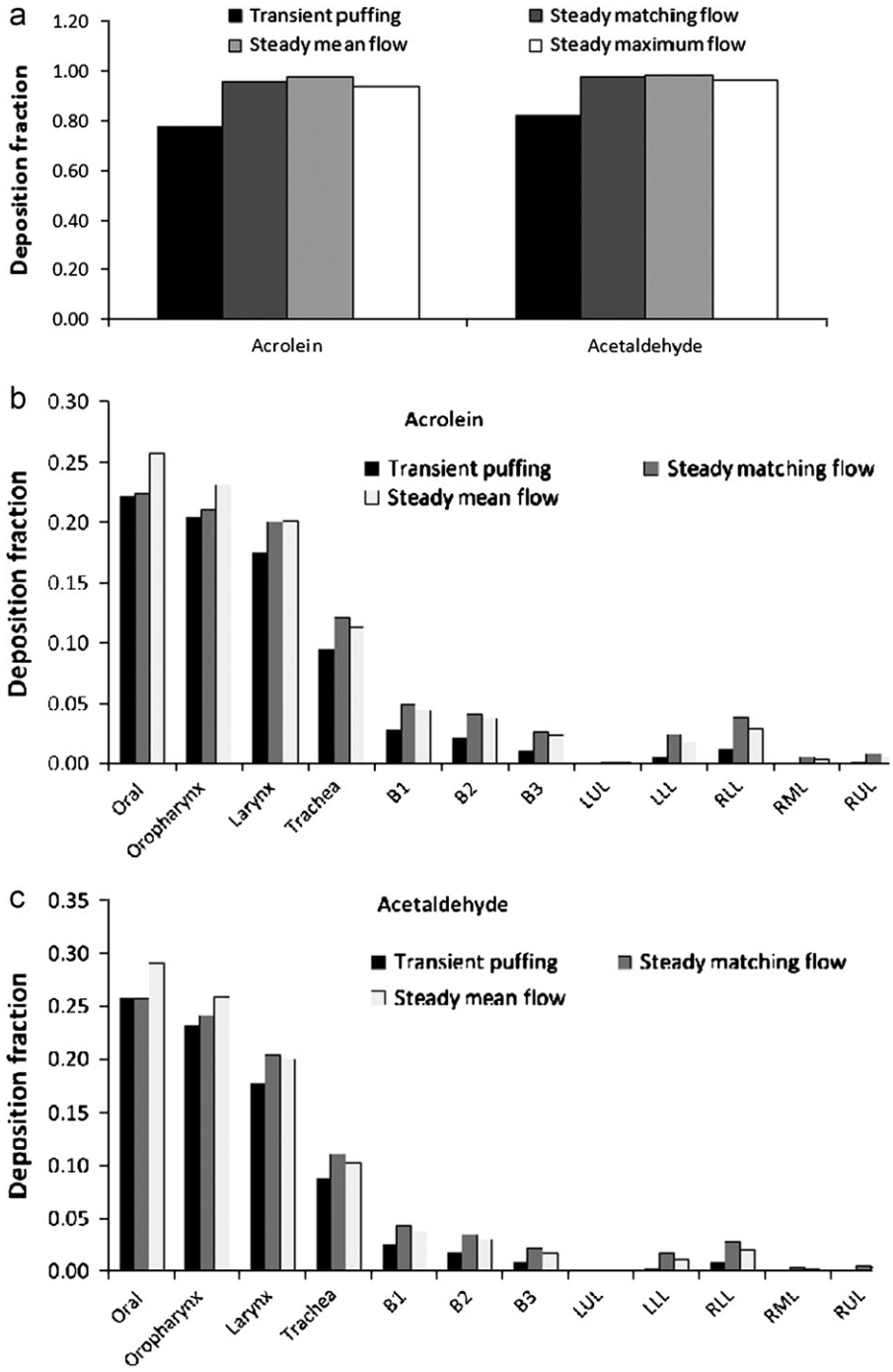

Fig. 9. Comparisons of deposition fractions for transient PREP puffing and at different constant flow rates: (a) Vapor deposition in the entire upper airway model; (b) acrolein vapor deposition in different airway regions; and (c) acetaldehyde vapor deposition in different airway regions.

Clearly, at the much higher velocities the delay times for vapors in various segments are much shorter when compared to just puffing, especially in the oral airways.

3.4. Deposition comparisons between steady and transient conditions

The total and regional deposition fractions of acrolein and acetaldehyde vapors in the upper airway model for transient puffing are compared with those for steady inhalation in Fig. 9. The matching flow rate is defined as the average between the mean and maximum flow rates, i.e., $Q_{match}=C(Q_{mean}+Q_{max})$ and C=0.5 (see Zhang and Kleinstreuer 2004). The values of different steady flow rates for different transient inhalation modes are given in Table 3.

As shown in Fig. 9, the total deposition fractions at three steady flow rates related to puffing are quite similar for two vapors, i.e., around 95% to 99%. But the deposition fractions under transient puffing are lower than those under steady inhalation conditions with three different flow rates, which are about 79% for acrolein vapor, and 83% for acetaldehyde. This is mainly due to the time delay for vapors penetrating deeper into the lung. This phenomenon can be further observed for regional deposition, as shown in Fig. 9b and c. Clearly, with larger time delay in the deeper lung region, the regional deposition fractions for transient puffing are much lower than those under corresponding steady flow conditions. Of special interest is the fact that deposition fractions in the oral cavity and oropharynx during *transient puffing* are very close to those when assuming *matching steady flow* values, rather than steady *mean* flow rates, as listed in Table 3. There are two reasons for this: (i) the time delays for vapor transport are short in the oral cavity and oropharynx (see Fig. 9b and c); and (ii) without the delay, the vapor deposition fraction over one inhalation cycle is closer to that for constant flow at the corresponding matching (pseudo-steady) flow rate than at the mean flow rate. Evidently, the momentary deposition fraction near the end of inspiration does not drop rapidly to zero as the flow rate does (see Fig. 9b and c).

A deposition correction factor (C_{DF}) is proposed to account for the reduced deposition at each airway region during transient puffing. Specifically, when assuming equivalent steady flow per cycle, the delay of vapor transport during transient flow results in the reduction of inhaled vapors in various regions. So, a correction factor can be employed to represent the reduced vapor concentration at the inlet for the specific region with transport delay, i.e.,

$$C_{DF}=1-\int_0^{t_{delay}} Q(t)Y_{in}(t)dt/\int_0^{T} Q(t)Y_{in}(t)dt \tag{13}$$

and

$$DF_{transient}=C_{DF}\cdot DF_{steady,match} \tag{14}$$

where t_{delay} is the delay time of vapors to the specific region (see Table 2) and T is the cycle period. Obviously, it is computationally very advantageous to run steady-state simulations, rather than transient ones, and obtain very similar vapor-deposition results. The correction factor and modified regional deposition fractions for two PREP vapors are given in Table 4. As expected, the modified deposition values based on the correction factor for the matching (steady) flow-rate case are very close to those under realistic transient puffing for most parts of the tract as well as the entire region.

Table 3
Corresponding steady flow rates for different transient cases.

Cases	Transient PREP puffing (Fig. 6)	Transient conventional cigarette (CC) puffing (Fig. 12)	Transient normal inhalation
Mean flow rate (mL/s)	37.5	30	500
Matching flow rate (mL/s)	51.4	58	643
Maximum flow rate (mL/s)	71.3	44	785

Table 4
Deposition correction factors and modified PREP regional vapor deposition.

Region	Correction factor	Acrolein vapor deposition			Acetaldehyde vapor deposition		
		Steady matching flow	Steady matching flow with correction	Transient puffing	Steady matching flow	Steady matching flow with correction	Transient puffing
Oral	0.985	0.2253	0.2219	0.2231	0.2588	0.2549	0.2588
Oropharynx	0.965	0.2119	0.2045	0.2050	0.2429	0.2344	0.2328
Larynx	0.897	0.2023	0.1815	0.1768	0.2057	0.1845	0.1787
Trachea	0.808	0.1219	0.0985	0.0964	0.1122	0.0907	0.0893
B1	0.593	0.0502	0.0298	0.0295	0.0445	0.0264	0.0265
B2	0.531	0.0425	0.0226	0.0221	0.0355	0.0188	0.0187
B3	0.42	0.0281	0.0118	0.0117	0.0225	0.0095	0.0096
B4–B9	0.4	0.0850	0.0340	0.0220	0.0600	0.0240	0.0160
Total		0.9672	0.8045	0.7866	0.9820	0.8431	0.8304

A relatively large difference still can be observed in the lower region B4 to B9, because a unique delay time and correction factor are employed for all individual bifurcations in the entire region of B4 to B9.

As shown in Fig. 10, the total and regional deposition fractions of acrolein and acetaldehyde vapors in the upper airway model for transient post-puffing (normal inhalation) are compared with those for steady inhalation as well. The situation differs measurably, depending on the mode of puffing. During normal transient inhalation, high flow velocities largely reduce the transport delay time of vapors into the deeper airways. The effect of transport delay is minor on both regional and total deposition in the upper airways from oral cavity to B9. Hence, both total and regional deposition fractions of vapors for cyclic inspiratory flow are very close to those for constant flow with the matching flow rate. As previously stated, vapor transport and deposition during transient inhalation are not synchronized with the variations in flow rate.

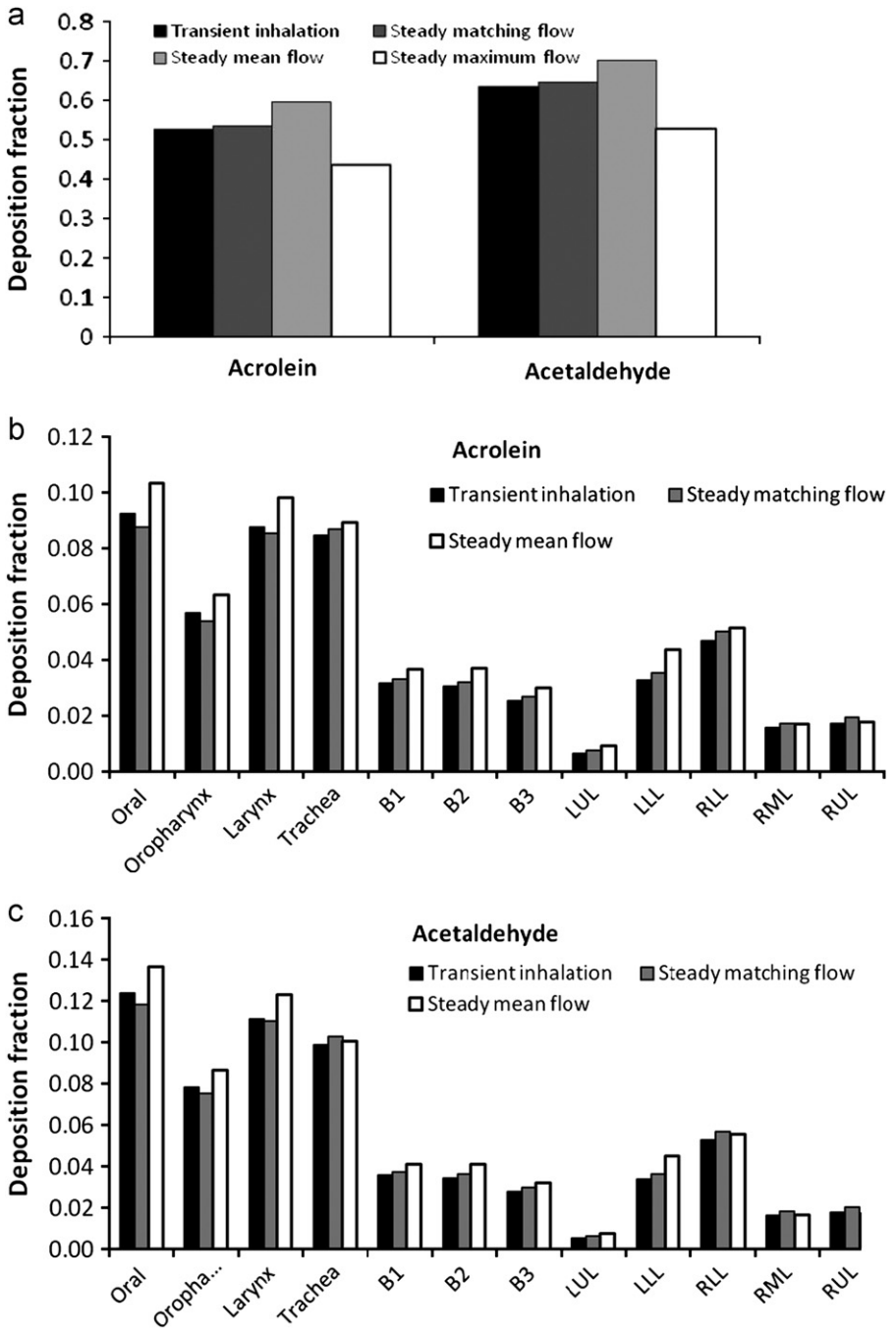

Fig. 10. Comparisons of deposition fractions for transient normal inhalation and constant flow with different flow rates: (a) Vapor deposition in the entire upper airway model; (b) acrolein vapor deposition in different airway regions; and (c) acetaldehyde vapor deposition in different airway regions.

For example, lingering vapors near the end of the inspiration cycle still deposit while the flow rate approaches zero (see Fig. 8). Such unsynchronized behavior causes the deposition fraction for transient inhalation to be different from the constant flow and vapor transport/deposition at the corresponding mean flow rate. It can also be seen from Fig. 10 that vapor deposition fractions for transient inhalation are lower than those for constant flow (at the mean flow rate) and higher at the maximum flow rate. However, the vapor deposition fractions for transient inhalation can be reasonably approximated when employing the matching flow rate approach. This is also consistent with previous studies for vapor deposition in the human nasal cavity (Shi et al., 2006), in an idealized human oral airway model (Zhang et al., 2004), and in nasal cavities of rats (Jiang & Zhao, 2010).

3.5. Deposition comparisons between PREP and CC vapors

There are two major differences for some PREP vapors and conventional cigarette (CC) vapors during transient puffing. The first is that the initial and inlet concentrations at the mouth inlet are different for PREPs and CCs. The second difference is the puffing waveform. The different inlet and initial vapor concentrations naturally influence actual vapor mass

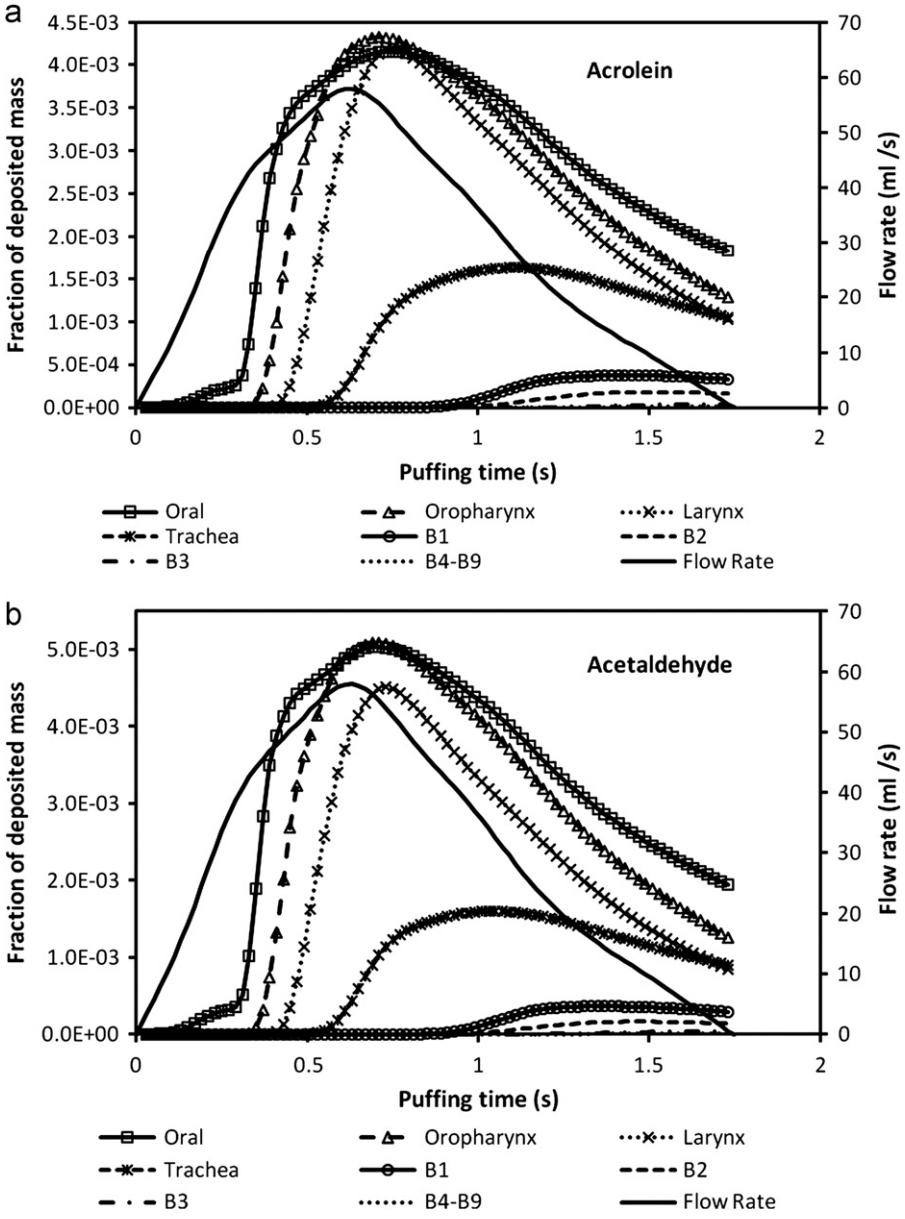

Fig. 11. Variations of momentary deposition fraction during one CC puffing cycle: (a) Acrolein vapor deposition in different airway regions; and (b) acetaldehyde vapor deposition in different airway regions.

depositing on airway wall surfaces; however, they may not affect the vapor deposition fractions. In this section the effects of puffing waveforms on total and regional vapor deposition fractions in the upper airway model are discussed.

Fig. 11 depicts a typical CC-puffing waveform (see Dickens et al., 2009) and the variation of momentary deposition fractions of acrolein and acetaldehyde vapors during one puffing cycle. Clearly, the relationship between the momentary deposition fraction and flow rate is similar for PREPs and CCs. However, the transport delay times (cf. Tables 5 vs. 2) are different because of different mean and maximum flow rates (see Table 3) as well as the puffing-time period. *Clearly, CC vapors cannot reach deeper airway regions,* i.e., *beyond B3.*

The deposition correction factors for CC-vapor deposition are given in Table 5 as well. Again, CC-vapor deposition fractions for transient puffing can be represented by the modified deposition values with correction factors for constant flow at the corresponding matching flow rate (see Table 6).

Fig. 12 compares regional deposition fractions of acrolein and acetaldehyde vapors under transient PREP- and CC-puffing conditions. Of interest is that the deposition fractions in the oral and oropharynx are close; although, the inhalation waveforms are quite different. This is because the deposition decrease, due to longer vapor transport delay, offsets the deposition increase due to a lower flow rate (i.e., longer residence time). However, beyond the larynx the vapor deposition fraction for CC puffing becomes lower and lower than for PREP puffing because the travel delay effect becomes more and more dominant. So, the total deposition fraction in the upper airways for transient PREP puffing ($DF_{\text{acrolein}}=79\%$, $DF_{\text{acetaldehyde}}=83\%$) is higher than for transient CC puffing ($DF_{\text{acrolein}}=68\%$, $DF_{\text{acetaldehyde}}=74\%$). In summary, compared with CC puffing, PREP puffing implies a higher flow rate and longer period. Hence, *the vapor can penetrate and deposit more in the deeper lung airways under transient PREP-puffing conditions.*

Table 5
Transport delay time of CC vapors in different airway regions.

Region	Oral	Oropharynx	Larynx	Trachea	B1	B2	B3	B4–B9
Delay time (s)	0.21	0.31	0.39	0.55	0.95	1.11	1.35	> 1.7
Correction factor	0.943	0.873	0.804	0.644	0.253	0.15	0.05	0

Table 6
Regional deposition of CC vapors under transient puffing and steady matching flows.

Region	Acrolein vapor deposition			Acetaldehyde vapor deposition		
	Steady matching flow	Steady matching flow with correction	Transient puffing	Steady matching flow	Steady matching flow with correction	Transient puffing
Oral	0.2411	0.2274	0.2251	0.2750	0.2593	0.2631
Oropharynx	0.2219	0.1937	0.1975	0.2517	0.2197	0.2237
Larynx	0.2041	0.1641	0.1637	0.2052	0.1650	0.1661
Trachea	0.1163	0.0749	0.0754	0.1058	0.0681	0.0726
B1	0.0493	0.0125	0.0122	0.0430	0.0109	0.0120
B2	0.0416	0.0062	0.0051	0.0341	0.0051	0.0048
B3	0.0268	0.0013	0.0008	0.0210	0.0011	0.0008
B4–B9	0.0748	0.0000	0.0003	0.0516	0.0000	0.0003
Total	0.9758	0.6801	0.6800	0.9874	0.7292	0.7433

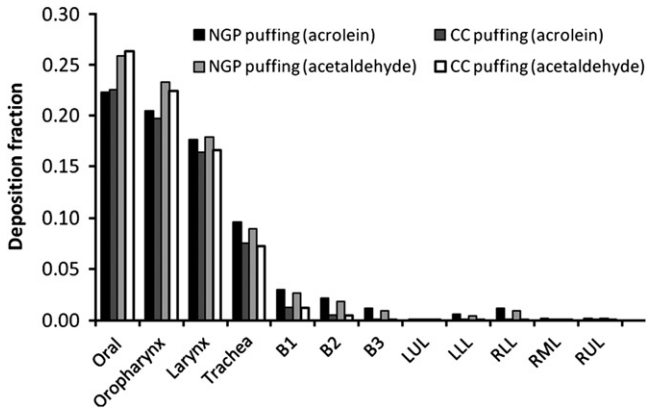

Fig. 12. Comparisons of regional vapor deposition fractions for transient PREP puffing and CC puffing.

3.6. Vapor deposition correlations

As given in Eq. (9), the vapor deposition efficiency (DE) in a given airway segment can be calculated as a function of species diffusivity in air, airway wall absorption coefficient, mass transfer coefficient, airway wall surface area, and local inlet flow rate. Hence, obtaining the respiratory mass transfer coefficient, h_m, is critical in quantitatively predicting the regional deposition of vapors. Traditionally, the mass transfer coefficient in terms of non-dimensional Sherwood number (Sh) is a function of Reynolds number (Re) and Schmidt number (Sc). Zhang & Kleinstreuer (2011a) developed a set of generalized $Sh = \text{fct.}(Re, Sc)$ equations based on a combined nasal-oral-tracheobronchial airway model for normal inspiratory flow rates. However, the oral and tracheobronchial airways in that study are not subject-specific, i.e., they were relatively idealized. Furthermore, the flow rates considered in Zhang & Kleinstreuer (2011a) are not in the puffing flow regimes. Hence, based on the present computer simulation data, the Sherwood-number for vapors of acrolein and acetaldehyde in different segments of subject-specific upper airways are also correlated as a function of local Reynolds numbers during puffing to post-puffing (see Tables 7 and 8). It should be noted that these correlations are for constant flows, and that the realistic deposition values can be inferred based on constant matching flows with time delay corrections.

Table 7
Correlation of Sh-number of acrolein vapor ($\tilde{D}_a = 0.105\ \text{cm}^2/\text{s}$) as a function of local inlet Reynolds number (Re) in segments of human upper airways.

Airway segment	Correlation equation [a]	r^2	Parameter range (Re)
Oral cavity and oropharynx	$Sh = 0.155Re^{0.7}$	0.992	100–3500
Larynx	$Sh = 0.221Re^{0.647}$	0.998	100–3500
Trachea	$Sh = 0.0768Re^{0.744}$	0.990	100–3500
B1	$Sh = 0.479Re^{0.536}$	0.993	100–3200
B2	$Sh = 0.521Re^{0.522}$	0.935	60–2500
B3	$Sh = 0.751Re^{0.473}$	0.918	30–2300
B4–9	$Sh = 0.577Re^{0.491}$	0.988	20–800

[a] Trachea diameter is considered as the characteristic length for segments of oral cavity, oropharynx, larynx and trachea; while diameter of parent tube is the taken as the characteristic length of the bronchial airway bifurcation.

Table 8
Correlation of Sh-number of acetaldehyde vapor ($\tilde{D}_a = 0.124\ \text{cm}^2/\text{s}$) as a function of local inlet Reynolds number (Re) in segments of human upper airways.

Airway segment	Correlation equation	r^2	Parameter range (Re)
Oral cavity and oropharynx	$Sh = 0.150Re^{0.7}$	0.995	100–3500
Larynx	$Sh = 0.203Re^{0.653}$	0.998	100–3500
Trachea	$Sh = 0.069Re^{0.747}$	0.988	100–3500
B1	$Sh = 0.470Re^{0.531}$	0.993	100–3200
B2	$Sh = 0.486Re^{0.523}$	0.939	60–2500
B3	$Sh = 0.725Re^{0.470}$	0.912	30–2300
B4–9	$Sh = 0.480Re^{0.517}$	0.992	20–800

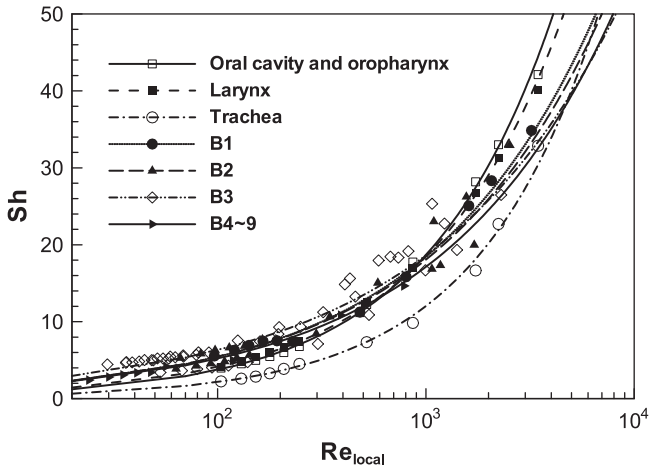

Fig. 13. Calculated Sherwood-number of acrolein vapor and correlation curves as a function of local Reynolds number in segments of human upper airways.

Fig. 13 depicts the $Sh-Re_{local}$ correlation curves and the simulated data points for acrolein vapor. The contribution of convection (i.e., *Re*-number) on mass transfer can also be observed from these graphs. Clearly, the stronger the convection (higher *Re*-numbers), the higher is the mass transfer. The flow structures and airway geometric features also have an important effect on vapor mass transport. Specially, the $Sh=Sh(Re)$-relationship may be different at various airway regions because of the interactions among local geometric features, flow turbulence (starting typically after the throat), and upstream deposition.

3.7. Effect of saturable pathway elimination

As mentioned in Section 2.2, the saturable pathway elimination can influence vapor absorption in the mucus and tissue layers. As described by the boundary conditions (2a), (4) and (5), vapor deposition with the saturable pathway elimination is dependent on the reaction and metabolism properties (e.g., K_f and K_m) of vapors in the tissue. Hence, the accurate simulation of vapor absorption with reaction and metabolism must be based on reliable properties. However, there are only a very few reaction/metabolism property data sets available for vapors of acteldehyde and acrolein, especially for humans. In fact, the Michelis-Menten parameters for the same vapor vary a lot in different publications. For example, Schroeter et al. (2008) argued that the best K_m-value for acrolein vapor in humans and rats is 0.5 mg/m^3, based on the match between their mass transfer simulations and measured deposition in rats. However, Mitchell & Petersen (1989) measured a K_m-value of acrolein vapor in rats being about 4600 mg/m^3.

Fig. 14 depicts the total deposition fraction of acetaldehyde vapor in the human upper airway model from mouth to generation G9 at a steady puffing rate of $Q=37.5$ mL/s. The reaction/metabolism properties used in these simulations are given in Table 9. As the inlet concentration increases, the tissue concentration increases as well. After the local/regional tissue concentrations reach the saturable plateau, the uptake of vapor at this region decreases. For acetaldehyde vapor under a puffing flow rate of 37.5 mL/s, the vapor deposition fraction drops about 13% when the inlet concentration increases from zero to 200 ppm. After that, the deposition hardly changes with the inlet concentration.

In the transient absorption process, the tissue concentration may not reach the saturable plateau as rapidly as in the quasi-steady case and the tissue concentration can also be depleted somewhat during exhalation and pausing (Asgharian et al., 2011). In this case, the effect of inlet vapor concentration on vapor deposition can decrease.

3.8. Limitations of the present study

As mentioned, in this study quasi-steady radial mass transfer in the mucus layer was employed, assuming the concentration below the mucus layer to be zero with rapid removal of vapor molecules by the underlying tissue. Recently, Tian & Longest (2010a,b,c) developed an air-mucus-tissue-blood (AMTB) boundary condition, which can predict different

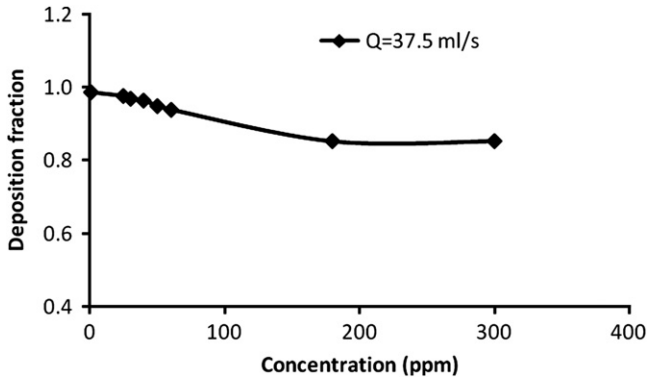

Fig. 14. Effect of inlet concentration on the total deposition of acetaldehyde vapor in the entire upper airway model (steady state, $Q=37.5$ mL/s).

Table 9
Reaction and metabolism properties of acetaldehyde vapor in human airways

K_f (s^{-1})	K_m (mg/m^3)	V_{max}/V_t (mg/m^3/s)	H_t (μm)	$\tilde{D}_t$ (cm^2/s)
0.03573 [a]	1320 [b]	1.214×10^{4} [b]	60 [c]	0.47×10^{-5} [d]

[a] Asgharian et al. (2012).
[b] Teeguarden et al. (2008).
[c] ICRP (1994).
[d] Calculated as one-third value of mucus (Tian & Longest, 2010b).

absorption concentrations in each layer for realistic transient flux conditions. In their first paper they also stressed that what is absorbed by the mucus may not be a good representation of tissue and blood exposures to the compound. In the follow-up paper, Tian & Longest (2010b) simulated the deposition of acetaldehyde vapor in an oral airway model from mouth to trachea. Their simulation results showed that the deposition fractions in the oral airway (under steady inhalation of 30 L/min) were 29.87% considering transient absorption conditions in mucus-tissue-blood layers. It has to be noted that they had used a rather low diffusivity of 0.08 cm^2/s. With the same diffusivity (0.08 cm^2/s) and air-mucus partition coefficient (320) as employed by Tian & Longest (2010b), the deposition from the mouth to the trachea in the present airway model with the present airway wall boundary condition is 28.22%. Clearly, this deposition value is very close to theirs for transient absorption in both mucus and tissue layers (29.87%); although, the geometries of the two studies were different. It implies that the present quasi-steady mucus absorption boundary condition is a good approximation of transient mucus-tissue boundary conditions in modeling vapor deposition in the mucus layer. In addition, Tian & Longest (2010b,c) also demonstrated that for a steady wall flux model, vapor absorptions in mucus, tissue and blood are all the same, which are dramatically different when transient flux is considered. It should be noted that for the steady multi-layer model of Tian & Longest (2010b,c), the airway wall absorption parameter K in the mucus layer was defined as $K=\tilde{D}_m/\tilde{D}_a\beta H_m(1-\tilde{C}_m)$ with $\tilde{C}_m=H_t\tilde{D}_m/\tilde{D}_a\lambda_{tm}H_m+H_t\tilde{D}_m$ and $\tilde{C}_m=0.9448$ for acetaldehyde vapor. However, in the present single mucus-layer model the absorption parameter K is $K=\tilde{D}_m/\tilde{D}_a\beta H_m$, which is much larger than that in the multi-layer model of Tian & Longest (2010b,c). The quite different K-values for steady flux conditions in these two studies result in a large difference of deposition in the mucus layer. However, to consider transient absorption of vapors during both inhalation and exhalation (Tian & Longest, 2010c) is helpful to more accurately predict the vapor deposition in air-mucus-tissue-blood system.

As discussed in Section 3.7, the airway wall absorption presented in Sections 3.2–3.6 can be reduced for cases of high inlet concentrations due to saturable pathway elimination. However, as indicated in Eqs. (2), (4) and (5), the vapor deposition with saturable pathway elimination is still a function of the airway wall absorption parameters K; but, the K-values change with the vapor reaction/metabolism properties in the tissue. As reported by Zhang & Kleinstreuer (2011a), the effects of K-values on respiratory mass transfer coefficients in the airways are minor. Hence, the correlations given in Tables 7 and 8 are still effective for estimating vapor deposition, considering saturable pathway elimination with reliable properties. In addition, this study focuses on the comparison of vapor deposition in the airway wall between steady and transient inhalation. The transient boundary conditions with or without saturable pathway elimination should not change the relationship between steady and transient vapor transport in the air and deposition from airway lumen to the wall. However, further studies are still required to investigate the interaction among patient-specific airway geometries, transient inhalation/exhalation of inhaled vapor, and transient absorption in patient-specific mucus-tissue-blood layer with reaction/metabolisms.

The limitations of this study include rigid airway walls and uniform pressure outlet conditions. Hence, effects of moving lung airways and more physiologically corrected outlet conditions will be considered in future studies.

4. Conclusions

The deposition of four selected tobacco-smoke vapors, i.e., acrolein, 1,3-butadiene, acetaldehyde and CO, in a subject-specific airway model under both transient puffing and post-puffing as well as constant flow conditions have been analyzed, employing a realistic and accurate computer simulation model. Both conventional cigarettes (CCs) and potential reduced exposure products (PREPs) with associated inhalation waveforms were considered. The following conclusions can be drawn:

Vapor deposition is strongly influenced by its property values. As almost insoluble species in the mucus layer, the deposition of butadiene vapor and CO is very low in the upper airways. The remaining vapors may penetrate further and deposit in deeper lung regions. As medium-to-high soluble vapors, acrolein and acetaldehyde have very large deposition values in the human upper airways, i.e., from mouth to generation G9. Specifically, the total deposition fractions in the upper airway model during single transient PREP puffing are about 79% for acrolein vapor and 83% for acetaldehyde vapor, ignoring the effect of saturable pathway elimination.

The deposition result for steady matching flow is a computationally efficient and good conservative estimate when compared to the actual deposition fraction under transient normal inhalation condition. However, the vapor transport delay may largely reduce vapor deposition for transient puffing. A correction factor has been proposed to incorporate vapor transport delay, in order to calculate efficiently actual deposition fraction values under transient puffing condition.

Compared to CC puffing, PREP puffing behavior may exhibit a higher flow rate and longer inhalation period. Hence, the vapor can penetrate and deposit more in the deeper lung airways during transient PREP puffing. Specifically, the total deposition fraction in the upper airways for a single transient PREP-puffing action (i.e., $DF_{\text{acrolein}}=79\%$, $DF_{\text{acetaldehyde}}=83\%$) is higher than for transient CC puffing ($DF_{\text{acrolein}}=68\%$, $DF_{\text{acetaldehyde}}=74\%$). It clearly implies that the puffing waveform can alter the local and regional vapor depositions.

A set of deposition correlations have been developed to estimate the deposition of acrolein and acetaldehyde vapors in different segments of the human upper airways under both puffing and normal inhalation (i.e., post-puffing) conditions.

Acknowledgments

This study was sponsored in part by Philip Morris Products S. A. (Neuchâtel, Switzerland). The authors are especially grateful for the support provided by Dr. Nveed Chaudhary (Manager of Disease Research and Biological Systems Research, Philip Morris Products SA). The use of both Fluent software from ANSYS Inc. (Canonsburg, PA) and IBM Linux Cluster at the High Performance Computing Center at North Carolina State University (Raleigh, NC) are gratefully acknowledged as well.

References

Asgharian, B., Price, O.T., Schroeter, J.D., Kimbell, J.S., Jones, L., & Singal, M. (2011). Derivation of mass transfer coefficients for transient uptake and tissue disposition of soluble and reactive vapors in lung airways. *Annals of Biomedical Engineering*, *39*, 1788–1804.

Asgharian, B., Price, O.T., Schroeter, J.D., Kimbell, J.S., & Singal, M. (2012). A lung dosimetry model of vapor uptake and tissue disposition. *Inhalation Toxicology*, *24*, 182–193.

Backhurst, J.D., & Martin, C.T. (1973). Retention of vapour phase constituents of cigarette smoke by the smoker—method development. BAT R&D Report L. 425-R. 〈http://tobaccodocuments.org/bw/17326.html〉.

Baker, R.R., & Dixon, M. (2006). The retention of tobacco smoke constituents in the human respiratory tract. *Inhalation Toxicology*, *18*, 255–294.

Bernstein, D.M. (2004). A review of the influence of particle size, puff volume, and inhalation pattern on the deposition of cigarette smoke particles in the respiratory tract. *Inhalation Toxicology*, *16*, 675–689.

Burns, D.M., Dybing, E., Gray, N., Hecht, S., Anderson, C., Sanner, T., O'Connor, R., Djordjevic, M., Dresler, C., Hainaut, P., Jarvis, M., Opperhuizen, A., & Straif, K. (2008). Mandated lowering of toxicants in cigarette smoke: a description of the World Health Organization TobReg proposal. *Tobacco Control*, 17.

Bush, M.L., Frederick, C.B., Kimbell, J.S., & Ultman, J.S. (1998). CFD-PBPK hybrid model for simulating gas and vapor uptake in the rat nose. *Toxicology and Applied Pharmacology*, *150*, 133–145.

Dickens, C., McGrath, C., Warren, N., Biggs, P., & McAughey, J. (2009). Puffing and inhalation behaviour in cigarette smoking: Implications for particle diameter and dose, in: *Inhaled Particles X*, Kenny L., ed.

Hecht, S.S. (2002). Cigarette smoking and lung cancer: chemical mechanisms and approaches to prevention. *Lancet Oncology*, *3*, 461–469.

Hecht, S.S. (2003). Tobacco carcinogens, their biomarkers and tobacco-induced cancer. *Nature Reviews Cancer*, *3*, 733–744.

Hecht, S.S., Yuan, J.M., & Hatsukami, D. (2010). Applying tobacco carcinogen and toxicant biomarkers in Product regulation and cancer prevention. *Chemical Research in Toxicology*, *23*, 1001–1008.

Horsfield, K., Dart, G., Olson, D.E., Filley, G.F., & Cumming, G. (1971). Models of the human bronchial tree. *Journal of Applied Physiology*, *31*, 207–217.

International Commission on Radiolocial Protection (ICRP), G. (1994). *Human Respiratory Tract Model for Radiological Protection, Annals of the ICRP*. Elsevier: New York ICRP Publication 66.

Jiang, J.B., & Zhao, K. (2010). Airflow and nanoparticle deposition in rat nose under various breathing and sniffing conditions—a computational evaluation of the unsteady and turbulent effect. *Journal of Aerosol Science*, *41*, 1030–1043.

Keyhani, K., Scherer, P.W., & Mozell, M.M. (1997). A numerical model of nasal odorant transport for the analysis of human olfaction. *Journal of Theoretical Biology*, *186*, 279–301.

Kleinstreuer, C., & Zhang, Z. (2010). Airflow and particle transport in the human respiratory system. *Annual Review of Fluid Mechanics*, *42*, 301–334.

Laugesen, M., & Fowles, J. (2006). Marlboro UltraSmooth: a potentially reduced exposure cigarette? *Tobacco Control*, *15*, 430–435.

Li, W., Xiong, J.Q., & Cohen, B.S. (1998). The deposition of unattached radon progeny in a tracheobronchial cast as measured with iodine vapor. *Aerosol Science and Technology*, *28*, 502–510.

Lin, S., Fonteno, S., Weng, J.H., & Talbot, P. (2010). Comparison of the toxicity of smoke from conventional and harm reduction cigarettes using human embryonic stem cells. *Toxicological Sciences*, *118*, 202–212.

Ma, B.S., & Lutchen, K.R. (2006). An anatomically based hybrid computational model of the human lung and its application to low frequency oscillatory mechanics. *Annals of Biomedical Engineering*, *34*, 1691–1704.

Menter, F.R., Langtry, R., & Volker, S. (2006a). Transition modelling for general purpose CFD codes. *Flow Turbulence and Combustion*, *77*, 277–303.

Menter, F.R., Langtry, R.B., Likki, S.R., Suzen, Y.B., Huang, P.G., & Volker, S. (2006b). A correlation-based transition model using local variables—Part I: Model formulation. *Journal of Turbomachinery—Transactions of the ASME*, *128*, 413–422.

Mitchell, D.Y., & Petersen, D.R. (1989). Metabolism of the glutathione-acrolein adduct, *S*-(2-aldehydo-ethyl)glutathione, by rat-liver alcohol and aldehyde dehydrogenase. *Journal of Pharmacology and Experimental Therapeutics*, *251*, 193–198.

Morris, J.B. (1996). Uptake of acrolein in the upper respiratory tract of the F344 rat. *Inhalation Toxicology*, *8*, 387–403.

Morris, J.B. (1997). Uptake of acetaldehyde vapor and aldehyde dehydrogenase levels in the upper respiratory tracts of the mouse, rat, hamster, and guinea pig. *Fundamental and Applied Toxicology*, *35*, 91–100.

Morris, J.B., & Blanchard, K.T. (1992). Upper respiratory—tract deposition of inspired acetaldehyde. *Toxicology and Applied Pharmacology*, *114*, 140–146.

Morris, J.B., & Hubbs, A.F. (2009). Inhalation dosimetry of diacetyl and butyric acid, two components of butter flavoring vapors. *Toxicological Sciences*, *108*, 173–183.

PMP (2010). Data sets provided by Philip Morris Products S. A. (Neuchâtel, Switzerland).

Schroeter, J.D., Kimbell, J.S., Gross, E.A., Willson, G.A., Dorman, D.C., Tan, Y.M., & Clewell, H.J. (2008). Application of physiological computational fluid dynamics models to predict interspecies nasal dosimetry of inhaled acrolein. *Inhalation Toxicology*, *20*, 227–243.

Shi, H., Kleinstreuer, C., & Zhang, Z. (2006). Laminar airflow and nanoparticle or vapor deposition in a human nasal cavity model. *Journal of Biomechanical Engineering-Transactions of the ASME*, *128*, 697–706.

Shi, H., Kleinstreuer, C., & Zhang, Z. (2008). Dilute suspension flow with nanoparticle deposition in a representative nasal airway model. *Physics of Fluids*, *20*, 013301.

Tan, F.P.P., Soloperto, G., Bashford, S., Wood, N.B., Thom, S., Hughes, A., & Xu, X.Y. (2008). Analysis of flow disturbance in a stenosed carotid artery bifurcation using two-equation transitional and turbulence models. *Journal of Biomechanical Engineering—Transactions of the ASME*, *130*, 061008.

Teeguarden, J.G., Bogdanffy, M.S., Covington, T.R., Tan, C., & Jarabek, A.M. (2008). A PBPK model for evaluating the impact of aldehyde dehydrogenase polymorphisms on comparative rat and human nasal tissue acetaldehyde dosimetry. *Inhalation Toxicology*, *20*, 375–390.

Tolman, T.W. (1973). The retention of carbon monoxide by cigarette smoker. BAT R&D Report RD. 1043-R. 〈http://tobaccodocuments.org/bw/17446.html〉.

Tian, G., & Longest, P.W. (2010a). Development of a CFD boundary condition to model transient vapor absorption in the respiratory airways. *Journal of Biomechanical Engineering—Transactions of the ASME*, *132*, 051003.

Tian, G., & Longest, P.W. (2010b). Application of a new dosimetry program TAOCS to assess transient vapour absorption in the upper airways. *Inhalation Toxicology*, *22*, 1047–1063.

Tian, G., & Longest, P.W. (2010c). Transient absorption of inhaled vapors into a multilayer mucus-tissue-blood system. *Annals of Biomedical Engineering*, *38*, 517–536.

Zhang, Z., & Kleinstreuer, C. (2004). Airflow structures and nano particle deposition in a human upper airway model. *Journal of Computational Physics*, *198*, *23*, 44–57.

Zhang, Z., & Kleinstreuer, C. (2011a). Deposition of naphthalene and tetradecane vapors in models of the human respiratory system. *Inhalation Toxicology*, *23*, 44–57.

Zhang, Z., & Kleinstreuer, C. (2011b). Laminar-to-turbulent fluid-nanoparticle dynamics simulations: model comparisons and nanoparticle-deposition applications. *International Journal for Numerical Methods in Biomedical Engineering*, *27*, 1930–1950.
Zhang, Z., & Kleinstreuer, C. (2011c). Computational analysis of airflow and nanoparticle deposition in a combined nasal-oral-tracheobronchial airway model. *Journal of Aerosol Science*, *42*, 174–194.
Zhang, Z., Kleinstreuer, C., & Hyun, S. (2012). Size-change and deposition of conventional and composite cigarette smoke particles during inhalation in a subject-specific airway model. *Journal of Aerosol Science*, *46*, 34–52.
Zhang, Z., Kleinstreuer, C., & Kim, C.S. (2006). Transport and uptake of MTBE and ethanol vapors in a human upper airway model. *Inhalation Toxicology*, *18*, 169–184.
Zhang, Z., Kleinstreuer, C., & Kim, C.S. (2008). Airflow and nanoparticle deposition in a 16-generation tracheobronchial airway model. *Annals of Biomedical Engineering*, *36*, 2095–2110.
Zhao, K., Scherer, P.W., Hajiloo, S.a., & Dalton, P. (2004). Effect of anatomy on human nasal air flow and odorant transport patterns: implications for olfaction. *Chemical Sense*, *29*, 365–379.